Proceedings of the ASME 2017 36th International Conference on Ocean, Offshore and Arctic Engineering
OMAE2017
June 25-30, 2017, Trondheim, Norway

OMAE2017-62314

ON TOWER TOP AXIAL ACCELERATION AND DRIVETRAIN RESPONSES IN A SPAR-TYPE FLOATING WIND TURBINE

Amir Rasekhi Nejad *
Erin E. Bachynski
Torgeir Moan
Center for Ships & Ocean Structures (CeSOS), and Center for Autonomous Marine Operations and Systems (AMOS)
Department of Marine Technology, Norwegian University of Science and Technology (NTNU)
NO-7491, Trondheim, Norway
Amir.Nejad@ntnu.no

ABSTRACT

Common industrial practice for designing floating wind turbines is to set an operational limit for the tower-top axial acceleration, normally in the range of 0.2-0.3g, which is typically understood to be related to the safety of turbine components. This paper investigates the rationality of the tower-top acceleration limit by evaluating the correlation between acceleration and drivetrain responses. A 5 MW reference drivetrain is selected and modelled on a spar-type floating wind turbine in 320 m water depth. A range of environmental conditions are selected based on the long-term distribution of wind speed, significant wave height, and peak period from hindcast data for the Northern North Sea. For each condition, global analysis using an aero-hydro-servo-elastic tool is carried out for six one-hour realizations. The global analysis results provide useful information on their own - regarding the correlation between environmental condition and tower top acceleration, and correlation between tower top acceleration and other responses of interest - which are used as input in a decoupled analysis approach. The load effects and motions from the global analysis are applied on a detailed drivetrain model in a multi-body system (MBS) analysis tool. The local responses on bearings are then obtained from MBS analysis and post-processed for the correlation study. Although the maximum acceleration provides a good indication of the wave-induced loads, it is not seen to be a good predictor for significant fatigue damage on the main bearings in this case.

INTRODUCTION

Floating offshore wind turbines (FWTs) hold great promise for harvesting the wind power resource in relatively deep water (>50 m). In order to realize this potential in commercial floating wind parks, reductions in the levelized cost of produced electricity are needed. The development of rational design criteria and operational limits will allow for more efficient - yet safe - floating offshore wind turbines. At present, there is a common practice in the industry to set a limit for the maximum axial acceleration on the tower-top in the range of $0.2g$-$0.3g$, even though this is not explicitly specified in the design codes. This limit has important consequences for platform design [1] as well as wind turbine control strategies [2].

An earlier study by authors [3] evaluated the correlation of the tower top axial acceleration and drivetrain load effects for a bottom-fixed offshore wind turbine. The maximum axial acceleration in the monopile offshore wind turbine, which was below $0.1g$, was found to be primarily a function of the tower motion, and the drivetrain design drivers - such as axial force, bending moment and the torque - were not necessarily correlated with the tower motion. Here, we examine the rationality of the nacelle axial acceleration limit with respect to the drivetrain responses of a floating wind turbine.

Based on the results of a previous study [4] of several 5 MW FWT designs (a TLP, two semi-submersibles and a spar), the spar was chosen for further examination due to its relatively large motion, axial force, and nacelle (or tower top) axial (i.e. along the

*Address all correspondence to this author.

rotor shaft) acceleration. This result is, of course, only a reflection of the specific designs and environmental conditions which were considered in the study, and not a general result for different types of FWT designs. For all FWT concepts, the tower top axial acceleration is the result of a combination of wind-induced forces on the tower and rotor, the wave-induced forces on the platform, and the resulting rigid-body and flexible deformations of the structure. Due to the complex load combinations, the maximum axial acceleration is not generally in phase with either the maximum wind-induced or wave-induced loads, although high axial acceleration can tend to indicate the presence of large wind and wave loads.

The question then becomes: is it rational to set an operational limit on the axial acceleration measured at the tower top for a floating wind turbine? This article tries to answer this questions by evaluating correlation and physical relationship between the maximum axial acceleration at the tower top and the load effects in the drivetrain. In an earlier work by Nejad et al. [4], it was shown that the main bearing(s) are most affected by the motions and loads on FWTs compared to land-based turbines. It was also found that the wave-induced motions are responsible for the increase in damage in the main bearings. Therefore, this study is focused on the main bearings.

A decoupled analysis approach is pursued in this paper. Results from the global analysis of the spar FWT in SIMO-RIFLEX-AeroDyn [5] are used as input to a multi-body system (MBS) model of the drivetrain and gearbox. In the following sections, the numerical models are first introduced, and then additional details regarding the environmental input and load effect post-processing are given. Global and local analysis results are then presented, and the approach of an operational acceleration limit is challenged.

TABLE 1. WIND TURBINE SPECIFICATION [6, 7].

Parameter	Value
Type	Upwind/3 blades
Cut-in, rated and cut-out wind speed (m/s)	3, 11.4, 25
Hub height (m)	90.0
Rotor diameter (m)	126
Hub diameter (m)	3
Rotor mass ($\times$1,000 kg)	110
Nacelle mass ($\times$1,000 kg)	240
Hub mass ($\times$1,000 kg)	56.8

TABLE 2. FLOATING PLATFORM CHARACTERISTICS.

Parameter	Value
Water depth (m)	320
Displacement (tonnes)	8227
Hull mass (tonnes)	7466
Draft (m)	120
Surge natural period (s)	129.5
Heave natural period (s)	31.7
Pitch natural period (s)	29.7
Yaw natural period (s)	8.2
Tower bending period (s)	2.1

MODELS

The spar wind turbine which was studied consists of the OC3 Hywind hull and tower, as defined by Jonkman [6], and the NREL 5 MW reference wind turbine [7]. As in previous work [4], a chain mooring system with delta lines and clump weights was applied to approximate the mooring system stiffness described in [6]. The wind turbine specification is provided in Table 1, while the overall characteristics of the floating platform are summarized in Table 2.

In the global analysis in SIMO-RIFLEX-AeroDyn [5], the hull was modeled using a rigid body, while the tower, blades, and mooring lines were considered as flexible components. A full dynamic solution of the mooring system (using bar elements) was included. The hydrodynamic loads on the hull included the excitation, added mass and damping from the first order potential; viscous forces according to Morison's equation; mean wave drift forces; and Newman's approximation for the difference-frequency wave excitation. The aerodynamic loading was based on blade element/momentum (BEM) theory for mean wind speeds at or below 9 m/s, and generalized dynamic wake (GDW) for higher mean wind speeds. The wind turbine control system is as defined in [6]: constant torque is applied above rated speed, and the blade pitch control parameters are adjusted to obtain a stable model. The simplified control system does not include any peak shaving, and allows for rather large variations in rotor speed and power for wind conditions above rated speed. The results from the global analysis (accelerations, velocities, positions, and internal loads at the tower top) are used as input to the multibody model of the drivetrain.

The 5-MW reference drivetrain [8] employed in this study includes a high speed gearbox with four-point support configuration. This configuration reduces the non-torque loading entering the gearbox. Most of the axial force induced by the thrust load is then supported by the main bearings. Gears and bearings are modelled in MBS as force-elements. Gear contact is modeled by

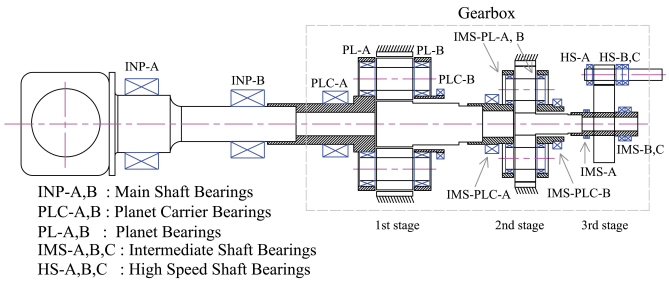

FIGURE 1. 5-MW REFERENCE GEARBOX LAYOUT [8].

TABLE 3. 5-MW REFERENCE GEARBOX SPECIFICATION [8].

Parameter	Value
Type	2 Planetary + 1 Parallel
1st stage ratio	1:3.947
2nd stage ratio	1:6.167
3rd stage ratio	1:3.958
Total ratio	1:96.354
Designed power (kW)	5000
Rated input shaft speed (rpm)	12.1
Rated generator shaft speed (rpm)	1165.9
Rated input shaft torque (kN.m)	3946
Rated generator shaft torque (kN.m)	40.953
Total dry mass ($\times$1000 kg)	53
Service life (year)	20

considering the profile modifications and lead corrections. Bearings are modeled with their stiffness and clearances.

The 5-MW reference gearbox used in this study was developed by Nejad et al. [8] for offshore wind turbines. This gearbox follows the most conventional design types of those used in wind turbines. The gearbox consists of three stages: two planetary and one parallel. Table 3 shows the general specifications of this gearbox. Fig. 1 shows the gearbox and drivetrain layout. The gearbox topology is also shown in Fig. 2. The gearbox was designed with a 4-point support with two main bearings to reduce non-torque loads entering the gearbox.

The MBS model of this gearbox is presented in Fig. 3. As shown, the motions are applied on the bed plate and the external loads on the main shaft. The generator torque and speed is then controlled at the generator side [8].

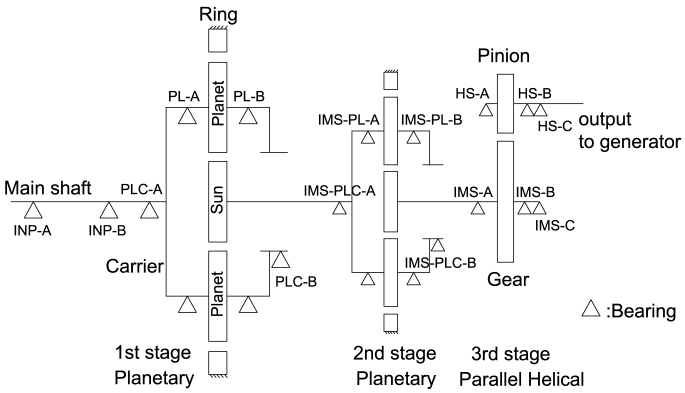

FIGURE 2. 5-MW REFERENCE GEARBOX TOPOLOGY [8].

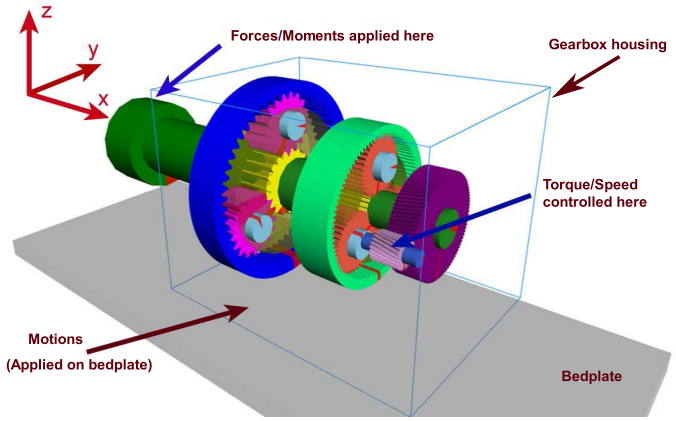

FIGURE 3. MBS MODEL OF 5-MW REF. GEARBOX [8].

METHODOLOGY

Dynamic response analysis & environmental conditions

A range of environmental conditions were selected based on the long-term wind-wave distribution for a representative site in the Northern North Sea (Site 14 in [9]). For wind speeds (U_w) within the operational range of the turbine, several combinations of significant wave height (H_s) and peak period T_p were selected based on the given conditional distributions (for H_s given U_w, and for T_p given U_w and H_s). For each wind speed in 1 m/s intervals, the combinations included:

1. the most probable H_s and corresponding most probable T_p,
2. the 90th percentile H_s and corresponding most probable T_p,
3. the 90th percentile H_s and corresponding 80th percentile T_p,
4. the 90th percentile H_s and corresponding 20th percentile T_p.

These conditions were not intended to allow for long-term study of the platform, but rather to provide a range of plausible conditions for which the connection between nacelle accelera-

TABLE 4. ENVIRONMENTAL CONDITIONS FOR DRIVETRAIN ANALYSIS.

EC	3	8	17	21	34	66	71	80	81	84
$U_w\ (m/s)$	6	11	20	24	16	6	11	20	21	24
$H_s\ (m)$	1.7	2.3	4.3	5.4	4.9	3.1	3.8	6	6.3	7.2
$T_p\ (s)$	9.5	10	11.3	11.9	11.7	9.2	9.7	11	11.1	11.6

tion and drivetrain responses could be studied. In all of the conditions, wind and waves are collinear, the turbine is operational, and no controller faults are considered. The different values of T_p provide a range of wave steepness. Fig. 4 shows the obtained 84 combinations of U_w, H_s, and T_p, as well as the maximum acceleration from 6 one-hour global analyses of each condition as a function of the wind speed. The choice of one-hour simulations is a compromise between 10 minutes (typically in the wind industry) and 3 hours (offshore), and has been shown to be reasonable [10].

As shown in Fig. 4, for the applied conditions, there is a strong correlation between the maximum acceleration and wind speed (a similar correlation, $r = 0.89$, can be shown between the maximum acceleration and H_s). The effect of wind and wave on the axial acceleration is discussed in the result section. The maximum obtained acceleration is around 0.31 g. Out of the 84 conditions in Fig. 4, 10 were selected for drivetrain analysis, as summarized in Table 4.

Bearing life

The main bearings in the 5 MW reference drivetrain are a CARB toroidal roller bearing for INP-A and one spherical roller bearing for INP-B [8] - see Fig. 1 for the nomenclature and the gearbox layout. The INP-A bearing carries the radial load and the axial force is supported by INP-B. This is a four-point drivetrain configuration, which significantly reduces the non-torque loadings that enter the gearbox [4, 11].

Bearings are designed based on the desired life expressed by [12]:

$$L = \left(\frac{C}{P}\right)^a \tag{1}$$

in which L is the bearing basic life defined as the number of cycles that 90% of an identical group of bearings achieve, under a certain test conditions, before fatigue damage appears. C is the basic load rating and is constant for a given bearing. The parameter a is given as $a = 3$ for ball bearing and $a = \frac{10}{3}$ for roller bearings, such as INP-A and INP-B. P is the equivalent

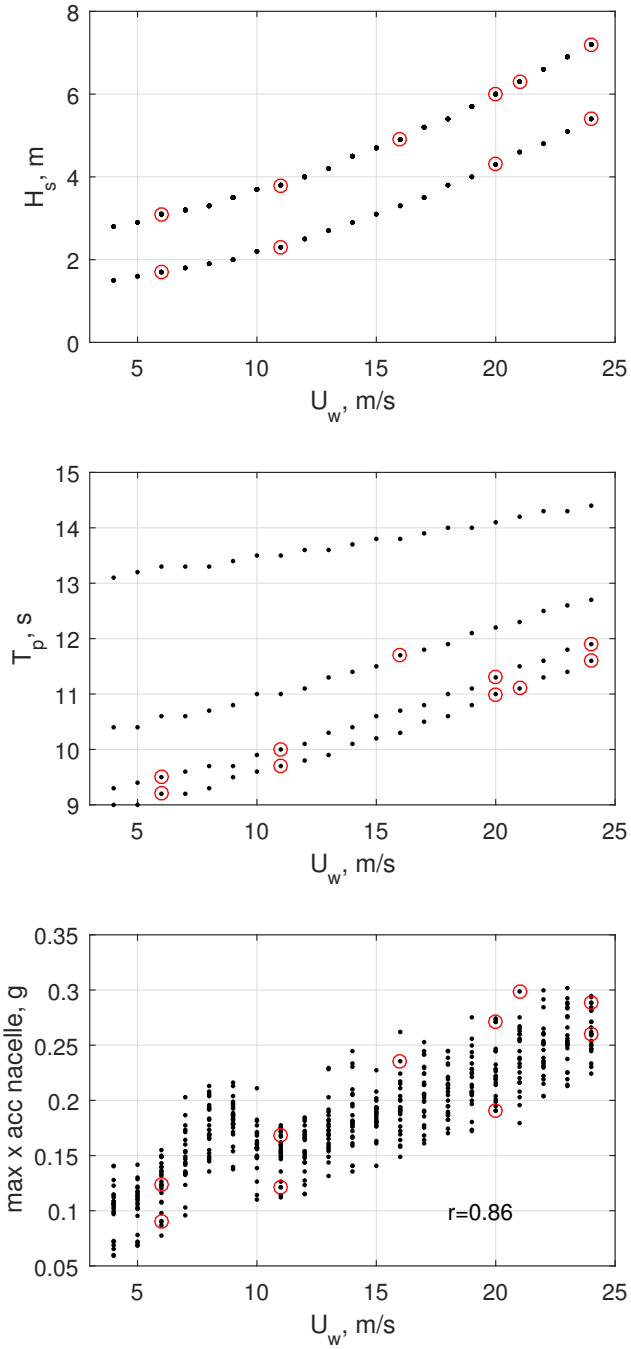

FIGURE 4. SCREENING OF ENVIRONMENTAL CONDITIONS. SELECTED CONDITIONS (RED CIRCLES) FOR DRIVETRAIN ANALYSIS ARE INDICATED.

radial or thrust load calculated from [13]:

$$P = XF_r + YF_a \tag{2}$$

where F_a and F_r are the axial and radial loads on the bearing respectively and X and Y are constant factors obtained from the bearing manufacturer. For INP-A, $X = 1.00$ and $Y = 0.00$, and for INP-B, $X = 0.67$ and $Y = 3.60$ respectively.

For time-varying loading, an equivalent steady load P_{eq} can be defined as [14]:

$$P_{eq} = \left(\frac{\sum n_i t_i P_i^a}{\sum n_i t_i} \right)^{\left(\frac{1}{a}\right)} \tag{3}$$

To apply this equation, the load duration distribution (LDD) method is employed [15]. In this method, the load is divided into a number of bins and the duration and speed associated with each bin is calculated. In Eq. 3, n_i is the rotational speed in bin i, t_i is the bin duration and P_i is the maximum load in that bin obtained from the equation 2.

As is evident from the formulation of bearing life in Eq. 1, P_{eq} is a good measure for comparing the bearing life in different environmental conditions. In the following section, P_{eq}, calculated for 1h, was used for the comparison.

RESULTS & DISCUSSIONS

Global load effects

In order to understand whether or not the axial acceleration can provide useful information about the load effects in the bearings, we begin by examining the characteristics of the tower top acceleration. Fig. 5 illustrates the frequency spectrum of the axial acceleration at the tower top. These results are obtained from the global analysis, but only the conditions which are applied in the local analysis are shown here for the sake of clarity. Despite the wide range of environmental conditions, one trend is clear: wave-induced forces have the biggest contribution in creating the axial acceleration, followed by effects near the 3P frequency (which may be related to tower shadow and turbulence effects in the wind excitation, which may in turn excite the first tower bending natural frequency). Note that for cases with below-rated wind speed, EC3 and EC66, the 3P and 6P frequencies are shifted to the left, and 9P can also be seen.

In addition to the frequency distribution of the acceleration, it is also relevant to examine whether conditions which lead to high accelerations also lead to large responses. Fig. 6 presents the 1-h maximum torque, axial force, tower fore-aft bending moment at tower top and base, and the radial force on INP-A versus the maximum axial acceleration on tower top. These results are obtained from the global analysis, where each of the 504 points

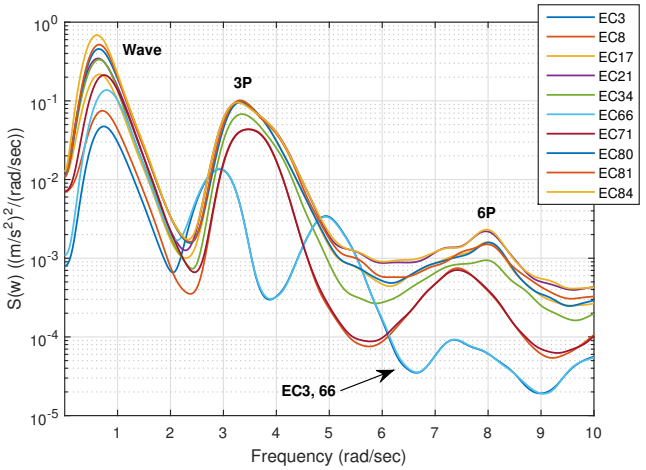

FIGURE 5. POWER SPECTRUM OF AXIAL ACCELERATION IN DIFFERENT ECs.

per response represents a single 1-hour simulation. The radial force on INP-A in Fig. 6 does not account for the drivetrain dynamics, but is merely taken as a combination of load effects from the global analysis.

In the first subplot, one can see that the one-hour maxima of torque and axial force are not linearly correlated with the one-hour maximum of axial acceleration. As expected and previously observed, the axial force follows the thrust force, and the effect of the blade pitch controller can clearly be seen above the rated wind speed for both the axial force and the generator torque [3].

In the second subplot, one can see that the one-hour maximum of the bending moment appears to be correlated with the maximum of the axial acceleration. As this bending moment is carried by the main bearings, consequently a similar correlation is observed for the radial force applied on the first main bearing, INP-A, in the third subplot. It should, however, be noted that the maximum axial acceleration and maximum moment do not necessarily occur simultaneously: one might hypothetically reach the threshold acceleration within a given storm after the structure has already suffered the maximum bending moment.

Although the bending moment at the tower base is not directly related to the drivetrain responses, it is included in Fig. 6 since this moment may also serve as an important design criterion. Since the inertial loads from the large mass of the rotor-nacelle-assembly are a significant contribution to the bending moment, it is not surprising to see a strong correlation between the axial acceleration and tower base bending moment. Shutting down the turbine would be expected to reduce the tower base bending moment in these conditions since the large mean component from the thrust force would be removed.

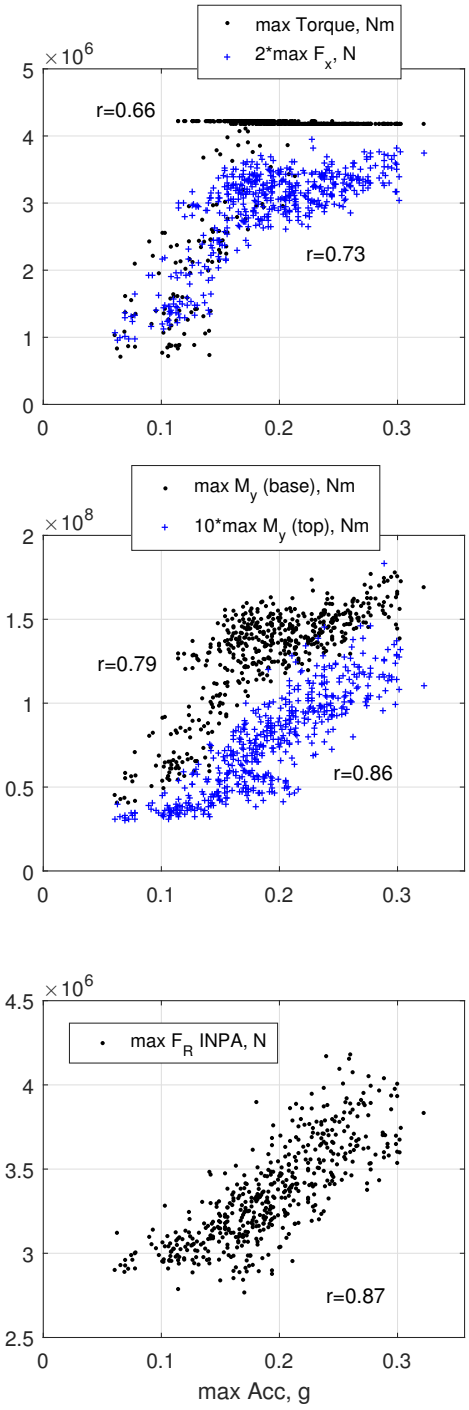

FIGURE 6. ONE-HOUR MAXIMUM TORQUE, AXIAL FORCE (F_x), TOWER FORE-AFT BENDING MOMENT (M_y) AT TOP AND BASE, AND LOAD ON BEARING INP-A, CORRELATED WITH ONE-HOUR MAXIMUM NACELLE ACCELERATION.

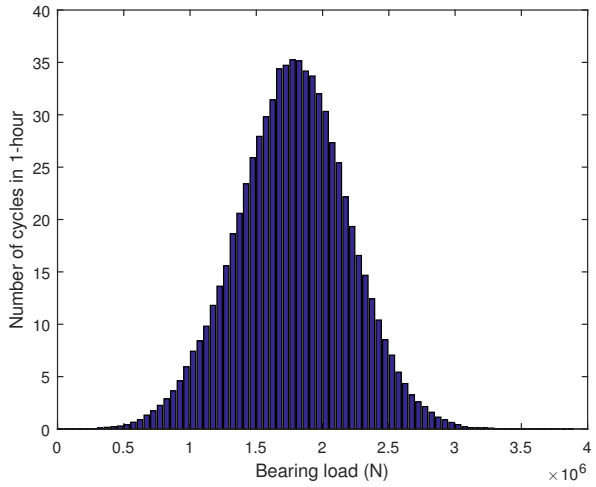

FIGURE 7. INP-A FORCE & NUMBER OF CYCLES, EC84.

Main bearing load effects

Next, the MBS results can be used to examine the load effects on the bearings, and how these are correlated with the one-hour maximum acceleration. Both the maximum loads and the equivalent fatigue loads must be considered.

Fig. 7 presents the radial load on INP-A versus the number of cycles in 1-h for EC84. From the ultimate limit design (ULS) perspective, the maximum load on this bearing is far lower than the acceptable dynamic load rating, C, recommended by the manufacturer. The same is true for the maximum force on INP-B (not shown), and one may therefore conclude that there is no issue with respect to the ULS design check. Normally, fatigue life is the design driver for bearings.

To evaluate the correlation between the fatigue life of these bearings and the maximum axial acceleration, the equivalent steady load P_{eq} for INP-A and INP-B are plotted in Fig. 8. Although one might hypothesize that continuing to operate during severe higher environmental conditions would have a significant effect on the life of these bearings, this does not appear to be the case.

It is interesting to observe that the highest P_{eq} for INP-B occurs at EC8 and EC71. These are the environmental conditions with wind speed of 11 m/s - see Table 4. This is the wind speed where the pitch control system becomes activated, and, due to the turbulent incoming wind, often switches between modes. The simple baseline controller is not ideal for these conditions, and the peak thrust force is reached here, which, together, leads to higher loads with a higher number of cycles and thus a higher fatigue damage. This also suggests that conditions around the rated wind speed are more crucial for the main bearings than more severe higher environmental conditions in terms of wind speed. Some improvement may be possible using a more sophisticated control algorithm, but the large thrust force will inherently affect

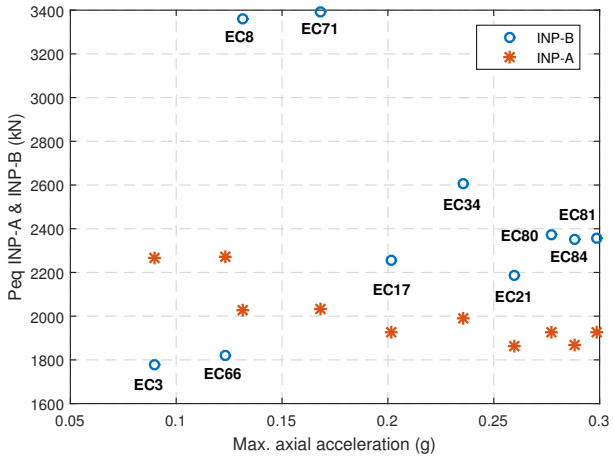

FIGURE 8. INP-A & INP-B EQUIVALENT STEADY LOAD (FOR FATIGUE LIFE) VERSUS MAX. AXIAL ACCELERATION.

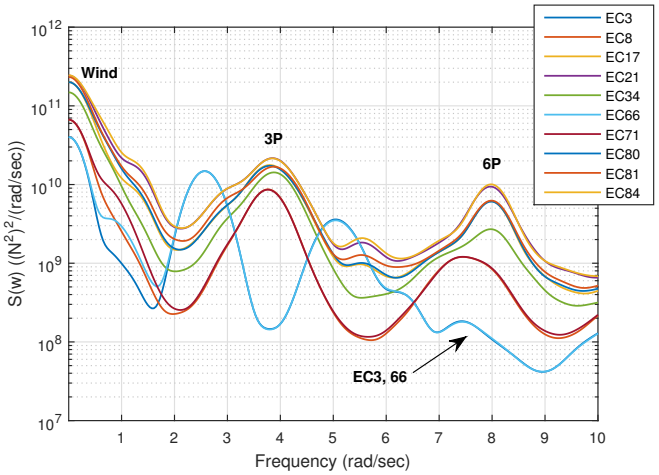

FIGURE 9. POWER SPECTRUM OF INP-A RADIAL FORCE IN DIFFERENT ECs.

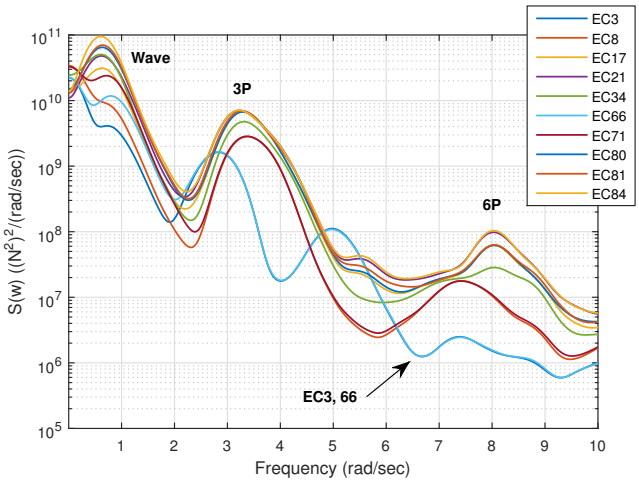

FIGURE 10. POWER SPECTRUM OF INP-B AXIAL FORCE IN DIFFERENT ECs.

the bearings' fatigue life.

Moreover, a negative trend is observed for the P_{eq} of INP-A in Fig. 8. Higher values are observed in lower wind speeds below rated due to relatively large loads with a high number of cycles, while for above rated the pitch control system is activated and the loading is limited.

In order to better understand the physical relationship between the axial acceleration and the bearing load effects, the frequency spectra of the INP-A radial force and INP-B axial force are shown in Figures 9 and 10. For INP-A, the wind-induced loads are the important components in the radial load: significant load effects at low frequency (turbulence in the wind) and at 3P (tower shadow and turbulence) can be seen. Comparing Fig. 9 with the spectrum of the axial acceleration shown in Fig. 5, it is found that axial acceleration is not a good measure for judging the loading on this bearing. The wave force is the dominant component in the axial acceleration while the radial force on INP-A is wind-dominated.

For the axial force on INP-B bearing, the effect of waves is evident in Fig. 10. One may, by comparing this figure with Fig. 5, conclude that the axial acceleration is a good measure to evaluate the maximum axial force on INP-B bearing since both are wave-dominated. This is, however, not a completely correct conclusion. The axial force on the bearing does not follow the axial acceleration but rather follows a constant pattern for the above rated wind speed as shown in Fig. 6. The reason is the fact that the axial force on the bearing is a combination of wave and wind forces. The wind part of this force is indirectly limited by the pitch control system, while the wave-induced part - which is transferred to the nacelle through the tower motion - is not. It is important to note that the wind part of the axial force is larger than the wave part for the case study spar. This can be seen in the earlier study by Nejad et al. [4] where the axial force on the land-based turbine (wind only) was compared with the axial force on the spar type floating wind turbine (wind and wave). As a consequence of this, the total axial force combining both wave and wind induced loadings, follows the pitch control system.

One may then ask: is the axial acceleration on the tower top a good measure to assess the wave part of the axial force on the bearing? To answer this question, first it should be noted that the type and size of the floating structure, mooring system and active or passive ballast system have a direct influence to limit the wave part of the axial force on the main bearing [4]. The wave-induced axial motion was much less in TLP and semi-submersible than in the spar studied in [4]. Whether the axial acceleration is a good or bad measure depends on the structure, but even in the case study spar with relatively large motions and large wave-induced

axial force, the near-rated wind speed conditions were found to be more critical than higher wind speed conditions for INP-B bearing life - see Fig. 8.

CONCLUSIONS

It is a common industrial practice to set a limit for the tower top maximum axial acceleration in floating wind turbines. In this paper, the rationality of this criterion was evaluated with respect to the drivetrain responses. A 5 MW reference drivetrain on a spar type floating wind turbine was used in this study. The global analysis was conducted using a state-of-the-art aero-hydro-servo-elastic tool for six one-hour realizations in 84 ECs. A decoupled analysis approach was employed to obtain drivetrain responses. For selected realizations, the load effects and motions from the global analysis were applied on a detailed drivetrain model in a MBS analysis tool. The local responses on bearings were obtained from MBS analysis and post-processed. The main bearings were selected for this study as they are the ones mostly affected by the motions of and loads on floating wind turbines compared with land-based turbines.

The results suggest that the wave-induced motion has the biggest contribution to the axial acceleration, followed by the tower shadow and turbulence effects at the 3P frequency.

From the global responses, the correlation between torque and axial force on the rotor and the maximum axial acceleration was investigated. It was found that the torque and axial force are mainly affected by the pitch control system, and are not correlated with the maximum axial acceleration.

The two main bearings were chosen for the drivetrain study. It was found that the fatigue life is the dominating parameter for the main bearings. A correlation was observed between the maximum tower top axial acceleration and the radial load on the first main bearing (INP-A) which carries the radial load only. However, the spectrum of the radial load on INP-A showed that wind and tower shadow are the dominant players, therefore, the correlation with the axial acceleration - which is wave-dominated - is not a good measure for judging the loadings on this bearing or its fatigue life assessment.

The second main bearing (INP-B) which carries the axial force was also investigated. The source of the axial force can be divided into the wind- and wave-induced loadings, where the wind part is controlled by the pitch system. Limiting the axial acceleration can be a good measure to control the wave induced loading part of the axial force on the main bearing. However, it was found that there are other environmental conditions with lower axial acceleration which reduce the fatigue life of the main bearings more than those with high axial accelerations.

Therefore, with respect to the main bearings, it was found that limiting the maximum axial acceleration may not be an efficient measure to make any conclusion about their maximum loadings or fatigue life.

It should be noted that there are limitations in this study: for instance, the applied wind turbine control system is a simple baseline model for research purposes, and the number and type of environmental conditions was limited. Future work is necessary to evaluate the effect of axial acceleration on other mechanical, electrical and electronic systems inside the nacelle.

ACKNOWLEDGMENT

The authors wish to acknowledge the financial support from Research Council of Norway through Center for Ships and Ocean Structures (CeSOS) and partially from Centre for Autonomous Marine Operations and Systems (AMOS-Project number 223254) at Department of Marine Technology, Norwegian University of Science and Technology (NTNU).

REFERENCES

[1] Zamora-Rodriguez, R., Gomez-Alonso, P., Amate-Lopez, J., De-Diego-Martin, V., Dinoi, P., Simos, A. N., and Souto-Iglesias, A., 2014. "Model scale analysis of a TLP floating offshore wind turbine". In ASME 2014 33rd International Conference on Ocean, Offshore and Arctic Engineering (OMAE2014), no. OMAE2014-24089.

[2] Goupee, A. J., Kimball, R. W., and Dagher, H. J., 2017. "Experimental observations of active blade pitch and generator control influence on floating wind turbine response". *Renewable Energy*.

[3] Nejad, A. R., Bachynski, E. E., Li, L., and Moan, T., 2016. "Correlation between acceleration and drivetrain load effects for monopile offshore wind turbines". *Energy Procedia,* ***94***, pp. 487–496.

[4] Nejad, A. R., Bachynski, E., Kvittem, M., Luan, C., Gao, Z., and Moan, T., 2015. "Stochastic Dynamic Load Effect and Fatigue Damage Analysis of Drivetrains in Land-based and TLP, Spar and Semi-Submersible Floating Wind Turbines". *Marine Structures,* ***42***, pp. 137–153.

[5] Ormberg, H., and Bachynski, E. E., 2012. "Global analysis of floating wind turbines: Code development, model sensitivity and benchmark study". In 22nd International Offshore and Polar Engineering Conference, Vol. 1, pp. 366–373.

[6] Jonkman, J., 2010. *Definition of the Floating System for Phase IV of OC3*. National Renewable Energy Laboratory.

[7] Jonkman, J., Butterfield, S., Musial, W., and Scott, G., 2009. Definition of a 5-MW reference wind turbine for offshore system development. Tech. Rep. NREL/TP-500-38060, US National Renewable Energy Laboratory (NREL).

[8] Nejad, A. R., Guo, Y., Gao, Z., and Moan, T., 2016. "Development of a 5 MW reference gearbox for offshore wind turbines". *Wind Energy,* ***19***(6), pp. 1089–1106.

[9] Li, L., Gao, Z., and Moan, T., 2015. "Joint distribution of environmental condition at five European offshore sites for design of combined wind and wave energy devices". *Journal of Offshore Mechanics and Arctic Engineering,* ***137***(3), pp. 031901–(1–16).

[10] Kvittem, M. I., and Moan, T., 2015. "Time domain analysis procedures for fatigue assessment of a semi-submersible wind turbine". *Marine Structures,* ***40***, pp. 38 – 59.

[11] Berger, B., 2016. Major component failure data & trends. Operations and Maintenance Summit Proceedings, 24-25 Feb. 2016, Toronto, Canada.

[12] IEC 61400-4, 2012. Wind turbines, part 4: Standard for design and specification of gearboxes.

[13] ISO 281, 2007. Rolling bearings - dynamic load ratings and rating life.

[14] Shigley, J. E., 2011. *Shigley's mechanical engineering design*. McGraw-Hill.

[15] Nejad, A. R., Gao, Z., and Moan, T., 2014. "On long-term fatigue damage and reliability analysis of gears under wind loads in offshore wind turbine drivetrains". *International Journal of Fatigue,* ***61***, pp. 116–128.